Received: 26 May 2021 | Revised: 18 August 2021 | Accepted: 23 August 2021

DOI: 10.1111/ejss.13165

ORIGINAL ARTICLE

European Journal of Soil Science WILEY

Soil aeration and redox potential as function of pore connectivity unravelled by X-ray microtomography imaging

Kristof Dorau[1] | **Daniel Uteau**[2] | **Maren Pia Hövels**[1] | **Stephan Peth**[3] | **Tim Mansfeldt**[1]

[1]Faculty of Mathematics and Natural Sciences, Department of Geosciences, Institute of Geography, University of Cologne, Köln, Germany

[2]Faculty of Organic Agricultural Sciences, Department of Soil Science, University of Kassel, Witzenhausen, Germany

[3]Institute of Soil Science, Faculty of Natural Sciences, Leibniz University Hannover, Hannover, Germany

Correspondence
Kristof Dorau, Faculty of Mathematics and Natural Sciences, Department of Geosciences, Institute of Geography, University of Cologne, Albertus-Magnus-Platz, D-50923 Köln, Germany.
Email: k.dorau@uni-koeln.de

Abstract

Platinum (Pt)-tipped electrodes are frequently employed to measure the soil redox potential (E_H). Thereby, the timely transition from reducing towards oxidising soil conditions is one of the most important biogeochemical changes that can occur in soil. This condition is mainly linked to the air-filled pore volume (ε) and pore geometries. However, even when the Pt electrodes are located in close vicinity to each other, E_H readings behave non-uniformly, presumably due to the millimetre scaled heterogeneity of pore spaces controlling oxygen (O_2) availability and transport. In this study, we examined the ε distribution and pore connectivity in the close vicinity of a Pt electrode during an artificial evaporation experiment using an undisturbed soil sample (Ah-horizon, Calcaric Gleysol). We combined physio-chemical methods with non-destructive X-ray computed microtomography (μCT) and 3D-image analysis. μCT scans were conducted at three-time points, that is, reducing conditions with $E_H < -100$ mV (CT-1), the transition from reducing towards oxidising conditions with an E_H increase > 5 mV h^{-1} (CT-2), and oxidising conditions with $E_H > 300$ mV (CT-3). We observed that the shift from reducing towards oxidising conditions took place at an air-filled porosity (ε_{CT}) of ~0.03 cm^3 cm^{-3}, which matches very with gravimetrically calculated data obtained by tensiometry of ε ~0.05 cm^3 cm^{-3}. Besides the relation of E_H and ε, image analysis revealed that a connected ε_{CT} (ε_{CT_conn}) of ~0.02 cm^3 cm^{-3} is needed to enable enhanced O_2 diffusion from the soil surface towards the Pt surface and facilitate a straightforward E_H response. We conclude that ε_{CT_conn} is a critical parameter to assess aeration processes in temporarily water-saturated soils to characterise a switch in redox conditions.

Kristof Dorau and Daniel Uteau contributed equally to this study.

Highlights

- Usually, soil redox dynamics are related to the air-filled porosity (ε_{CT}) but here its connected portion (ε_{CT_conn}) was found more relevant.
- 3D X-ray computed microtomography imaging close to a redox electrode enabled us to understand the soil aeration process.
- Connected ε_{CT} (ε_{CT_conn}) of ~0.02 cm^3 cm^{-3} facilitated oxidising soil conditions.
- ε_{CT_conn} is a critical parameter to assess the aeration process in temporarily water-saturated soils.

KEYWORDS

air-filled pore connectivity, air-filled pore volume, environmental monitoring, image analysis, redox potential, soil aeration, soil heterogeneity, X-ray computed microtomography

1 | INTRODUCTION

The transition from reducing towards oxidising soil conditions—referred to as soil aeration or oxygenation—is one of the most important chemical changes in soils (Glinski & Stepniewski, 1985). Usually, a platinum (Pt) electrode is installed in the soil to measure the redox potential (E_H) as an indicator of the redox status (Bohn, 1971). The E_H measurement has been encouraged for over a century (Gillespie, 1920), but it was a long way to gain knowledge on how to obtain E_H data and establish a proper functioning monitoring system for time-resolved and automated E_H measurements. However, E_H is known to vary considerably on a temporal (minutes to days) and spatial scale (millimetres to several metres), which renders a particularly complicated interpretation (Fiedler et al., 2007). In this regard, attempts to characterise the physio-chemical soil environment that is in contact with the Pt surface are scarce. Recent statistical approaches to quantify biogeochemical heterogeneity derived from a multitude of E_H readings are more than welcome (Wanzek et al., 2018). One approach to characterise the aeration status was proposed by Dorau et al. (2018), where undisturbed soil samples were equipped in parallel with Pt electrodes to record the E_H and micro tensiometers for the soil matric potential and thereupon calculate the air-filled pore space (ε). The authors identified soil-specific ε threshold values that characterise the ecologically important shift from anaerobic to aerobic soil microbial metabolism. Two characteristic ε values were defined: (i) $\varepsilon_{Pt\ reaction}$ indicated an initial diffusion of O_2 to which the Pt surface reacted (E_H increase > 5 mV h^{-1}) and (ii) $\varepsilon_{Pt\ aeration}$ enabled the assessment of the aeration status in terms of O_2 availability (E_H > 300 mV at pH 7) (Dorau et al., 2018). These dramatic transitions from reducing towards oxidising soil conditions occur, for example, when water tables drop, perched water tables disappear, or irrigation is finished. The main issue and omnipresent problem in soil science relates to scaling, that is, ε is not measured at the same location where the Pt-tip is positioned and, thus, the local pore geometry is neglected. Thus far, this problem continues to be a black box where input (i.e., changes in ε) is decoupled from the output (i.e., measured E_H).

A suitable method to map the pore geometry and combine soil physical properties with geochemical behaviour is X-ray computed microtomography (μCT) (Withers et al., 2021). Technological breakthroughs within the last 20 years enabled to visualise and quantify the geometry of the pore space via μCT (Peth et al., 2008; Pot et al., 2015). For instance, Tippkötter et al. (2009) and Carminati et al. (2008) demonstrated that it is possible to separate the air- and water-phase within the pore space. Pot et al. (2015) have directly measured pore-scale water configuration at high resolution and demonstrated model predictions of local water-gas phase interfaces using a lattice-Boltzmann approach (Pot et al., 2015). The three-dimensional distribution by water and air-filled pores has profound impact on soil reducing conditions, because O_2 diffusion coefficients were drastically curtailed by five orders of magnitude due to water filled-pores (Rohe et al., 2021). Thus, the electrode responds to changes in ε in close vicinity of the Pt surface because it further influences the electron availability due to the presence or absence of O_2. Non-destructive μCT imaging is a promising technique to observe 4D structural changes in ε during soil aeration, for example, visualise the spatial distribution of air-filled pores in close vicinity of a Pt electrode during soil aeration and its change in time.

This pilot study aims to shed light on the E_H–ε relation during the anaerobic–aerobic transition and explore this *terra incognita* interface. Thus, the objectives of this

study can be summarised as follows: (i) test the applicability of μCT to visualise the pore geometry in close vicinity of the Pt tip surface (a few cm^3) and (ii) assess the $E_H - \varepsilon$ relation via 3D reconstruction of ε during the soil aeration process. Therefore, we set up an incubation experiment and monitored on high temporal resolution (every 10 min) the E_H and ε within an undisturbed soil sample (a 250 cm^3 steel cylinder; Ah-horizon, Calcaric Gleysol). At discrete time points, μCT measurements complemented the dataset by providing an in situ pore network characterisation to achieve a 4D model of air-filled connected pore space.

2 | MATERIALS AND METHODS

2.1 | Soil sampling and properties

We obtained an undisturbed soil sample for the incubation experiment from a Calcaric Gleysol (Eutric) (IUSS Working Group WRB, 2015) located at Polder Speicherkoog in north Germany (54°8′1″N; 8°58′28″E). The site features a strongly fluctuating water table that favours the onset of temporarily reducing soil conditions within weeks, a prerequisite to study redox dynamics and soil aeration as exemplified by previous studies (Dorau & Mansfeldt, 2016; Mansfeldt, 2003, 2004). Prior to soil sampling, the grass cover was removed and a 250 cm^3 steel cylinder (50 mm height and 80 mm Ø) was pushed into the topsoil from 2 to 10 cm below ground. Afterwards, a polyethylene foam box was wrapped around the cylinder to minimise the collapse of the soil structure during transport to the laboratory. Soil properties were determined with air-dried and 2 mm-sieved material as follows: soil pH was measured potentiometrically with 0.01 M $CaCl_2$ solution mixed 5:1 with soil (v/v), the texture by wet sieving and settling method, total carbon, organic carbon (OC) and inorganic carbon (IC) by dry combustion with a CNS analyser (Vario EL cube, Elementar, Langenselbold, Germany), and finally $Mn^{III,IV}$ and poorly crystalline Fe^{III} oxides with oxalate (Schwertmann, 1964) and total Fe^{III} oxides which were extracted by dithionite–citrate–bicarbonate (Mehra & Jackson, 1960). The concentration of elements in the extracts were measured by flame atomic absorption spectroscopy (iCE 3000 series, Thermo Scientific, Waltham, MA).

2.2 | Water retention curve and air-filled pore volume

Multiple water retention curves of soil samples from the same study site and the same depth have been obtained in a previous study. A detailed description can be found in Dorau et al. (2018), which is also the conceptual and experimental basis for this study in conjunction with μCT 3D-image-analysis. We used the evaporation method with an HYPROP device (UMS, Munich, Germany) that measures a decrease in matric potential during evaporation of an initial water-saturated soil sample by two mini-tensiometers (5 mm Ø). The test assembly was used to derive the water retention function and for the redox experiment. It is placed on a balance to gravimetrically record changes in water content in 10 min intervals. We fit the data to the Durner equation (Durner, 1994) because it resulted in the lowest root mean square error for our retention data ($\theta_{RMSE} < 0.01$):

$$S_e = w_1\left(1+(a_1 h)^{n1}\right)^{-m1} + w_2\left(1+(a_2 h)^{n2}\right)^{-m2} \quad (1)$$

where S_e is the effective water content (−), w_1 and w_2 are weighting factors for two overlapping regions, and a_1, a_2, n_1, n_2, m_1 and m_2 are empirical fitting parameters for the hydraulic function. Based on the obtained hydraulic parameters during the incubation experiment, we calculated volumetric water contents (θ; $cm^3\ cm^{-3}$) and thereupon the air-filled porosity (ε; $cm^3\ cm^{-3}$) as:

$$\varepsilon = \theta_s - \theta, \quad (2)$$

with θ_s being the volumetric water content at saturation ($cm^3\ cm^{-3}$).

2.3 | Experimental setup and E_H measurements

The soil sample within the steel cylinder was gently pushed out by a customised stamp into a same-sized plastic container to enhance X-ray transmission through the sample. Then, the plastic cylinder was saturated by capillary force in a water bath containing a 0.01 M $CaCl_2$ solution (instead of distilled water) to minimise osmotic stress for microorganisms. After 1 week of saturation, we cautiously set the HYPROP device upside down on to the soil sample and then turned the test assembly upside down. A customised plastic lid was sealed by silicone gel on top of the plastic ring, which contained three boreholes: (a) one at 2 cm from the cylinder border for a redox Pt electrode (ecotech, Bonn, Germany with a tip 5 mm length and 1 mm Ø), (b) one at 4 cm from the first hole for the reference electrode (SE23, Sensortechnik Meinsberg, Waldheim, Germany) and (c) and one hole in the middle to aerate the sample on demand. We inserted both electrodes through the lid until they were 25 mm

below the sample's surface and sealed the aeration hole with a rubber plug. We did not correct the measured E_H to pH 7 in terms of comparability (Bohn, 1971) because a neutral soil reaction is present for the study site. Thus, all E_H values refer to pH 7 in the following when not specifically mentioned.

2.4 | µCT image acquisition

Samples were scanned at distinct time points using an X-ray microtomograph (Zeiss Xradia Versa 520, Carl Zeiss Microscopy GmbH, Jena, Germany) with an X-ray energy of 130 keV. The time points are referred to as CT-1, CT-2 and CT-3 and feature the following states: CT-1 was conducted as soon as a steady-state of E_H was reached under strongly reducing conditions with $E_H < -100$ mV, CT-2 reflects the transition from reducing towards oxidising conditions with an E_H increase >5 mV h^{-1} and CT-3 denotes oxidising conditions with $E_H > 300$ mV. Subsequent to CT-1, the rubber plug was removed from the aeration port and the soil water was allowed to evaporate and aerate the soil over time. However, we sealed the aeration port during the CT-2 and CT-3 measurement to prevent loss of soil water and water redistribution within the porous network and to guarantee that the acquired µCT images are characteristic for the in situ soil water content and thereupon ε. The timing to conduct the measurements was based on empirical evidence by a previous study, where aeration curves have been established with soil samples from the same study site (Dorau et al., 2018). Hence, there was some degree of uncertainty because of the difficulty to control the physio-chemical behaviour of the soil system to match the prerequisites stated above. The cabling of the HYPROP device was disconnected during the µCT measurements to close the X-ray chamber, thus, no E_H and ε data was recorded for a few hours.

At each time point, we scanned two regions of interest (ROI), first an overview scan with 172 cm^3 after the image reconstruction and second, a close-up of 2.55 cm^3 containing the Pt tip at the centre. The reconstructions achieved a voxel edge length of 39.4 µm for the overview and 14.4 µm for the close-up. A summary of scanning parameters is shown in Table S1.

2.5 | Image pre-processing and analysis

Image analysis of the reconstructed 3D datasets was done with MAVI (Modular Algorithms for Volume Images, Fraunhofer ITWM, Kaiserslautern, Germany) implemented in a Framework called ToolIP, where numerous 3D analytical solutions can be automatised by means of flow processing charts. Renderings were done with Paraview 5.7 (Kitware Inc., New York, NY). On the overview scan dataset, a radial grey value gradient in the images was corrected slice-wise by converting the coordinates from cartesian to polar and applying a complementary mean gradient mask. Afterwards both images (overview and close-up) were spatially twofold binned and filtered using a median filter with window size 3^3 voxels to reduce noise and streak artefacts produced by the Pt electrode. We used Otsu's algorithm (Otsu, 1979) to separate the soil matrix from resolved pores in a new binary image. The original image was multiplied with the binary image to obtain the greyscale image of the pores, which was segmented again to separate air from water-filled pore space. We had to mask out about 3 mm around the Pt electrode in the overview image, because of streak artefacts that did not allow a classification of this region. For the close-up image, this was reduced to 2 mm from the Pt electrode surface.

At each time step, we quantified the resolved porosity, which was limited to pores with a diameter greater than 28.2 µm in the close-up and 78.9 µm in the overview images. To distinguish this from the gravimetrically calculated ε, we named it 'CT derived air-filled porosity' (ε_{CT}, cm^3 cm^{-3}). Furthermore, on the overview images we quantified ε_{CT} that was connected to the upper end of the sample, as O_2 would only be able to diffuse from the top of the sample where the aeration port was installed (Figure S3). To do that, we inverted the image so that the ε_{CT} became the foreground and added 10 foreground slices on the top of the image. Then, we labelled every macropore and filtered by a volume threshold so that all disconnected macropores (mostly entrapped air bubbles) were removed. Then, we removed the 10 foreground slices from the top. We called this 'connected air-filled porosity' (ε_{CT_conn}). Next, we applied radial masks around the Pt electrode with increments of 1.58 mm up to a distance of 50.48 mm where we quantified ε_{CT} and ε_{CT_conn}.

3 | RESULTS AND DISCUSSION

3.1 | Soil aeration assessed via tensiometric readings

Depending on dissolved O_2 concentration subsequent to water saturation, the microorganisms switch their metabolism from aerobic to anaerobic (Reddy & DeLaune, 2008) and caused a steep decline in E_H from 250 mV towards <−100 mV within 60 h (Figure 1a). This behaviour is typical for microbially active soils, as it is the case for the sample from Polder Speicherkoog, with nearly neutral soil reaction (pH 7.1), an OC content of 28.6 ± 0.92 g kg^{-1} and some

remaining IC with 2.1 ± 1.31 g kg^{-1}. Manganese and Fe oxide act against a change in E_H near the surface of the redox electrode by acting as redox buffering compounds but contents of 607 mg kg^{-1} and 8.22 g kg^{-1} did not hamper the rapid decrease (Table S2). This process is analogous to 'buffering capacity' with respect to the soil pH (Reddy & DeLaune, 2008). After removing the rubber plug from the aeration port to allow water to evaporate, the E_H remained reductive for 14 days. Then, it drastically increased from −170 to 640 mV from the CT-2 time step onwards (Figure 1a). Air-filled pores at CT-1 were absent as indicated by tensiometric readings during saturated conditions, but as soon as the water started to evaporate, the ε increased to 0.060 cm^3 cm^{-3} at CT-2 (Figure 1b). Subsequent to CT-2, the increase in ε was slowed down and reached 0.096 cm^3 cm^{-3} at the end of the experiment. The soil temperature fluctuated only marginally throughout the period and was on average 25.3 ± 1.22°C (Figure 1c).

The Pt electrode indicated an E_H response during our predefined CT-2 measurement with an $\varepsilon_{\text{Pt reaction}}$ value of 0.055 cm^3 cm^{-3} (Figure 1d). However, it took some days to aerate the region near the surface of the Pt electrode and to achieve oxidising soil conditions with a $\varepsilon_{\text{Pt aeration}}$ value with E_H ~300 mV of 0.066 cm^3 cm^{-3}. Hence, the switch from reducing towards oxidising soil conditions took place within the air-entry region of the soil close to water saturation (Figure S1). These values are close to the ones previously reported with 0.048 ± 0.008 for $\varepsilon_{\text{Pt reaction}}$ and 0.085 ± 0.007 cm^3 cm^{-3} for $\varepsilon_{\text{Pt aeration}}$ from the same study site (Dorau et al., 2018). Besides the overall linkage between ε and E_H, Nakamura et al. (2018) demonstrated the benefit from these kind of pedotransfer functions to water management practices, for example, when ε is known but data about reduced and toxic species in soil solution is missing. They found that dissolved arsenic (As) was only appreciable when ε was smaller 0.04–0.06 cm^3 cm^{-3} at a plot that featured a similar particle size distribution compared with our study. In another study, root elongation rate of radiata pine seedlings was close to zero at $\varepsilon < 0.05$ cm^3 cm^{-3}, a finding that was independent of soil texture (Zou et al., 2001). This indicates that a similar tipping range in ε indicated the transition from reducing towards oxidising soil conditions since As was rapidly immobilised (Nakamura et al., 2018) and root elongation was enhanced by invading O_2 above the ε threshold (Zou et al., 2001).

3.2 | Soil aeration assessed via 3D reconstruction of air-filled pores

Pre-selected timing to conduct the µCT scans was on empirical evidence and indeed, the defined prerequisites

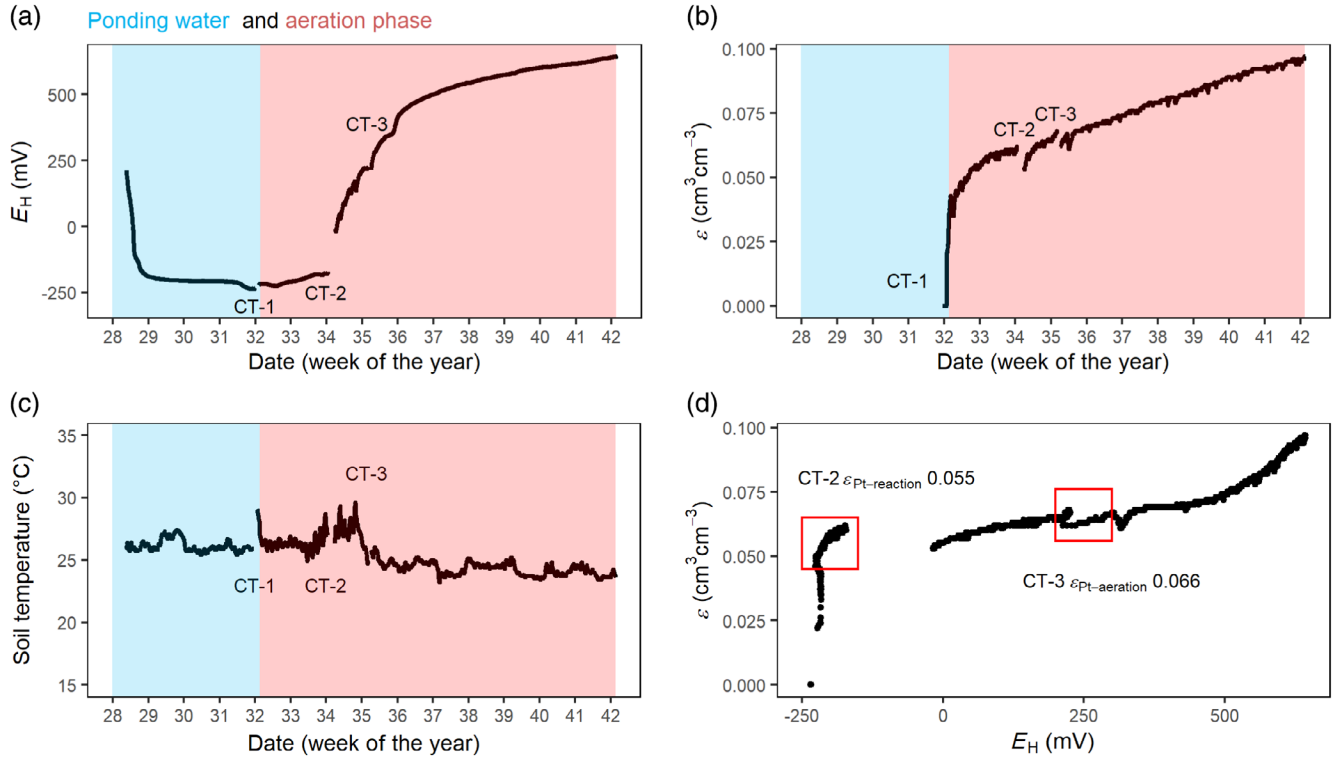

FIGURE 1 Development of redox potential (E_H; a), air-filled pore volume (ε; b), and soil temperature (c) during the 3 month incubation experiment. The time steps where the sample was measured by X-ray computed microtomography (µCT) are annotated with CT-1, CT-2 and CT-3 in each figure. The relation between E_H and ε (d) includes the characteristic tipping point $\varepsilon_{\text{Pt reaction}}$ (E_H increase >5 mV h^{-1}) and $\varepsilon_{\text{Pt aeration}}$ (E_H > 300 mV; red boxes)

matched. The first scan (CT-1) was done under strongly reducing conditions, CT-2 was conducted during the E_H increase due to changes in electron availability (i.e., O_2 enters the ROI) and CT-3 slightly before oxidising soil conditions with 250 mV (Figure 1). In the close-up during CT-1, all pores were water-saturated, but in the overview we could observe 0.039 cm^3 cm^{-3} of ε_{CT} (Figure 2 and Table 1), which indicates the presence of entrapped air bubbles (Figure S2A). From the Pt electrode readings, we presume the entrapped voids were composed of the redox-sensitive trace gases CO_2, N_2O and CH_4 rather than O_2. This remains speculative because the Pt surface only indicates the presence of a distinct species when being in contact with it and the air bubbles still might contain very low amounts of O_2. Based on the long incubation time we assumed equilibrium state between the entrapped bubbles and the surrounding environment and thus a high probability of an O_2-free environment. For both ROIs, the ε_{CT} gradually increased with time but was generally lower in the close-up compared with the overview (Table 1). This is mainly due to the slight compaction produced by inserting the electrode into the soil. Thereby, the comparison between ε_{CT} and ε thresholds to indicate the anaerobic-aerobic transition worked better in the overview compared to the close-up (Figure 2). The overview, with a volume of 172 cm^3 (Table S1), reflected better the response of the micro tensiometers and the retention characteristics, which are based on the 250 cm^3 cylinder (Figure S1), than the close-up with 3.24 cm^3. Clay contents of 250 ± 12 g kg^{-1} in the sample favoured coarse aggregation and, thus, a highly heterogeneous soil environment. This is relevant as the ε_{CT} and its connectivity to the free atmosphere are closely related to the macroaggregation of the soil. Such features determine the individual response of the Pt electrode during soil aeration.

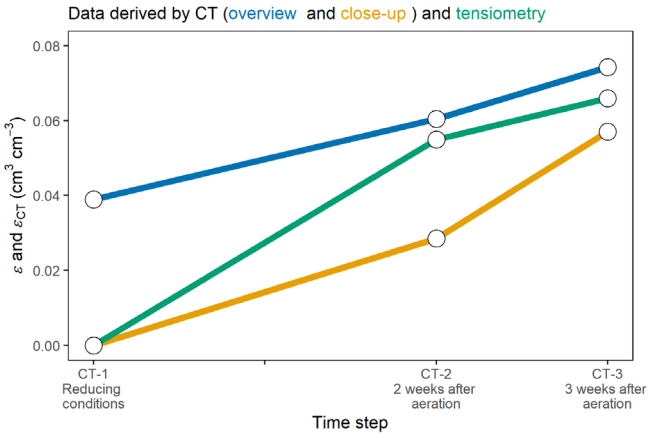

FIGURE 2 Development of the computed microtomography (CT)-derived air-filled porosity (ε_{CT}) for the overview and the close-up and the gravimetrically calculated ε for the three-time steps CT-1 (reductive), CT-2 ($\varepsilon_{Pt\ reaction}$) and CT-3 ($\varepsilon_{Pt\ aeration}$)

3.3 | Pore connectivity and O_2 pathways

Spatial dependence of E_H measurements exists at the microscale (Yang et al., 2006) and is an omnipresent issue to interpret the individual behaviour of redox electrodes even when being placed in close vicinity to each other. The spatial distribution of ε_{CT} in the overview scan during CT-1 fluctuated considerably from 0.020 to 0.065 cm^3 cm^{-3} (Figure 3a). In CT-2 and CT-3, ε_{CT} increased gradually to 0.059 ± 0.013 and 0.079 ± 0.015 cm^3 cm^{-3}, respectively (Figure 3d). An even better indicator to assess the response of the redox electrode is the ε_{CT_conn}. No ε_{CT_conn} was present in close vicinity of the Pt electrode surface during CT-1, which agreed very well with strongly reducing conditions and $E_H < -100$ mV indicating the absence of O_2 (Figure 3a). Undeniably, if the Pt electrode tip would have been placed at 27 mm in radial distance to the current position, a connected ε_{CT_conn} with 0.055 cm^3 cm^{-3} would not foster a retarded response of the E_H increase (14 days between CT-1 and CT-2; Figure 1a). The

TABLE 1 Properties of the computed microtomography (CT)-derived air-filled porosity (ε_{CT} and ε_{CT_conn}) from the pre-defined time steps CT-1, CT-2 and CT-3 for the overview of the sample and the close-up around the Pt redox electrode

	CT-1		CT-2		CT-3	
	Overview	Close-up	Overview	Close-up	Overview	Close-up
ε_{CT} (cm^3 cm^{-3})	0.0389	0	0.0605	0.0285	0.0743	0.0571
Surface to volume ratio (cm^2 cm^{-3})	31.5	—	32.5	93.3	35.1	101.6
ε_{CT_conn} (cm^3 cm^{-3})	0.0156	—	0.0380	—	0.0564	—
Ratio of the four biggest air-filled pores to the ε_{CT} (%)	40.4	—	55.2	49.4	56.4	51.0
Euler density of the sample (num cm^{-3})	12.8	—	11.8	101.4	12.4	−412.8
Euler number of the four biggest pores (−)	−4	—	−90	−89	−241	−950

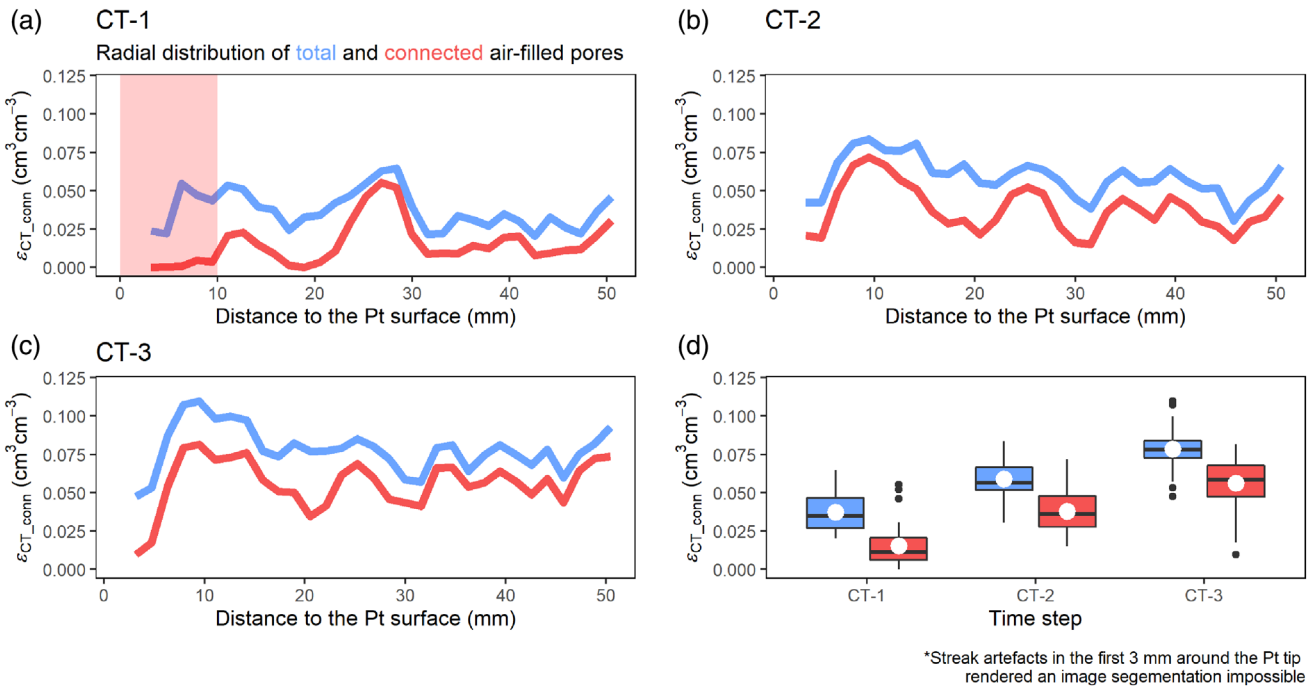

FIGURE 3 Transects of total and connected computed microtomography (CT)-derived air-filled porosity (ε_{CT} and ε_{CT_conn}, respectively) for the analysed time points CT-1 (a), CT-2 (b) and CT-3 (c) shown as distance to the surface of the redox electrode. The data is summarised in boxplot diagrams in d

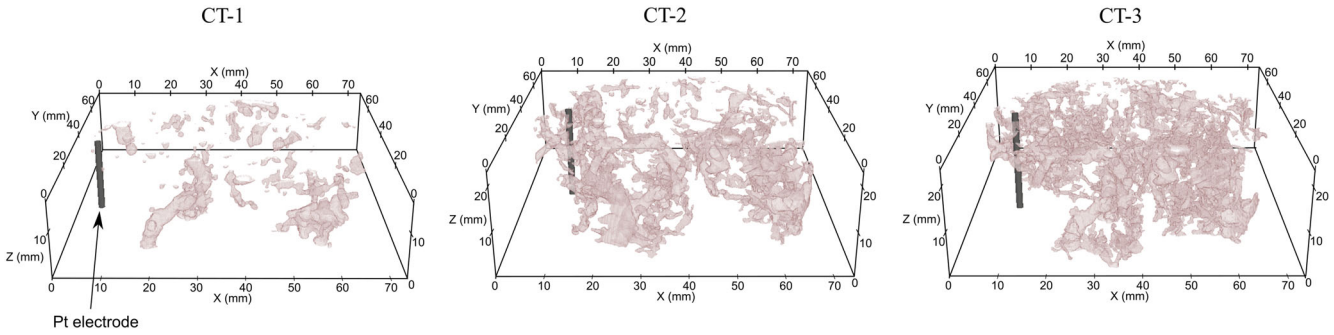

FIGURE 4 Connected CT-derived air-filled porosity (ε_{CT_conn}) on the overview images of the three-time steps: CT-1 (reductive), CT-2 ($\varepsilon_{Pt\ reaction}$) and CT-3 ($\varepsilon_{Pt\ aeration}$)

ROI around each Pt electrode surface is affected by the defined physical framework, which determines O_2 diffusion paths between the soil surface and the sampling site (Flühler et al., 1976). A critical threshold during CT-2, the moment were the redox electrode indicated aeration, was 0.020 cm^3 cm^{-3} ε_{CT_conn}, which enabled a continuous pathway for O_2 from the soil surface towards the Pt electrode surface (Figures 3b and 4). This occurred near to the air-entry value of the soil, which is characterised by the tension at which atmosphere air enters the soil. The improvement of the continuity of ε_{CT} is also shown in the ratio of the largest pores to the total ε_{CT}. In the close-up this goes from CT-1 having no ε_{CT}, to CT-2 where 49.4% was taken by the four largest pores, and to CT-3 where it increased to 51.0% (Table 1). Not only the continuity increased but also the connectivity improved at the same time which is shown by the Euler density turning from positive (many isolated pores) in CT-2 to negative (few isolated pores with many self-connections) in CT-3 (Table 1). The E_H response was straightforward as it is exemplified in Figure 5a. However, common examples frequently observed when E_H is measured in the field are shown in Figure 5b,c. A plausible explanation is a disrupted and discontinuous O_2 pathway in B from day 8 to day 15, where O_2 diffusivity equalled O_2 consumption and E_H reached quasi-stationary conditions at 100 mV. Redistribution of soil water within the porous network or rainfall events with seepage might be responsible for this

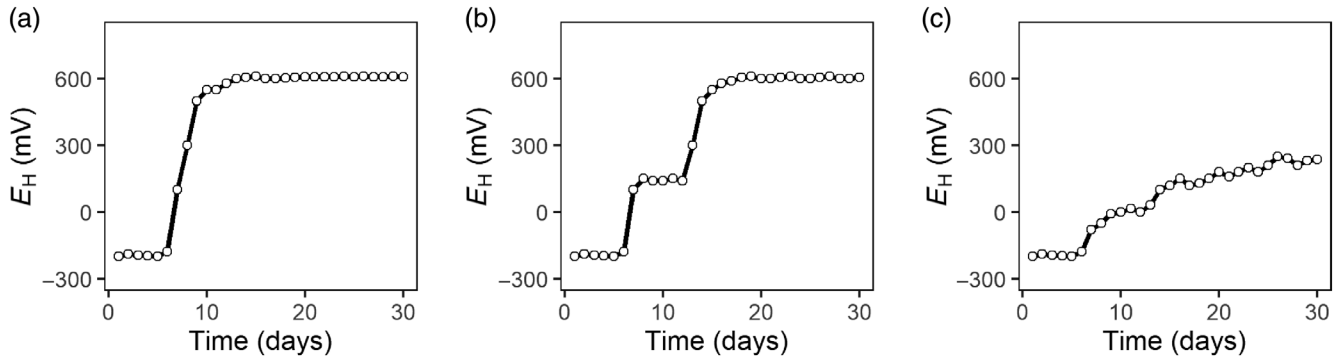

FIGURE 5 Hypothetical examples of aeration events assessed by the redox electrode. The examples are based on preliminary field work. Presumably, the different aeration curves are due to elevated (a), intermediate (b) and low (c) oxidative capacity (e.g., the volume, connectivity and oxygen (O_2) concentration of air-filled pores). This study exemplifies type A, elevated oxidative capacity, with air-filled pores that are interconnected and a short pathway from the Pt surface towards the soil surface (25 mm; O_2 reservoir of 100%)

pattern. Sometimes, blocking of pores might be enhanced such that a redox electrode does not measure an abrupt change in electron availability indicated by a steep E_H increase (Figure 5c). Overall, the relation between ε_{CT_conn} and E_H is not applicable for an indefinite period of time. Soils are in a continuous change and prone to management practices. As recently shown, conversion of degraded soils from bare fallow management towards arable or grassland increased the connected porosity significantly dependent on the input of SOC (Neal et al., 2020). Bare fallow soils, which have the lowest connected porosity, featured the highest anoxic proportion at field capacity (~30%) compared with arable (~10%) and grassland soils (~5%) (Neal et al., 2020). This highlights the important role of ε_{CT_conn} to control the anaerobic–aerobic transition during the soil aeration process, a process vulnerable by management practices on a decadal scale.

3.4 | Beneficial use and restrictions to study soil aeration by µCT

Non-invasive imaging techniques have made significant progress in recent years to study dynamic 3D soil pore spaces (Peth, 2014), as exemplified within this study. However, a bottleneck for soil aeration studies still remains as we were not able to resolve pores in the plant's available water range. Nevertheless, our study takes place in the air capacity range while thinner pores remained water saturated (Figure S1). Thus, we can neglect O_2 diffusion as it is 10^5 times reduced in the water phase (Rohe et al., 2021). Our technical equipment in conjunction with the large bulk soil volume of 250 cm^3 enabled us to quantify the ε_{CT} within pores up to 15 µm. Unfortunately there were processes that we could not account for, like the O_2 consumption rate, microbial activity and non-resolvable SOM, all of them intrinsic factors that control the E_H response. Keiluweit et al. (2018) integrated non-invasive O_2 imaging by planar optodes in combination with µCT achieving a voxel resolution up to 3.25 µm. In contrast to our setup, they used a repacked soil sample with a volume of around 13 cm^3. Such compromises have to be made to increase resolution. Since redox reactions are predominantly driven by microorganisms, a high and prolonged radiation by X-rays may have an impact on the microbial community structure. Fischer et al. (2013) found significant damage to specific microbial communities after a high X-ray radiation dose, however, they also observed a strong regeneration of microbial life and a recovery of bacterial community structure 1 week after µCT scanning. In our study we could not detect changes (indirectly) in microbial communities related to pure oxidising or reducing activity. Thus, we can confidently assume that only a minor impact occurred and the shift towards oxidising conditions was driven by the ε_{CT_conn} transporting O_2 from the surface of the sample.

Another issue resulting from the massive structure of the Pt electrode is the presence of streak artefacts resulting from the hardening of the X-rays because of its high density. Even using a Tungsten filter to harden the beam was not enough to get rid of this problem. An alternative could be to use gold and graphite electrodes that feature lower densities (19.3 and 2.26 g cm^{-3}, respectively) than platinum. However, gold has only a small equilibrium exchange current (i_0) of 10^{-9} A cm^{-2} and behaves poorly in natural media (Whitfield, 1972). The much lower density of graphite (2.26 g cm^{-3}) might be a good solution to overcome this problem. Further redox experiments bridging the gap between redox and CT measurements might employ O_2 microsensors in parallel, as they evoke less streak artefacts (Rohe et al., 2021). Nevertheless, as shown

in Uteau et al. (2015) there is a considerable delay in the microbial response to O_2 shortage, thus, the best alternative would be to monitor E_H together with O_2. This will be further pursued by the authors.

Overall, additional analysis across soils with variable structure (soil physical framework) and biogeochemical properties (labile OC and microbial communities) are needed to generalise critical ε_{CT} and ε_{CT_conn} values. This does not only refer to the composition of the soil sample but also to the representative volume and the number of replicates that are considered. As shown by Wanzek et al. (2018), soil pore network metrics to predict redox dynamics were dependent on scale. Thereby, the smallest volume of interest (VOI) with 190 mm^3 had the greatest power to statistically explain changes in E_H compared with 25 and 100 cm^3 VOI. Thus, the suggestion by Fiedler et al. (2007) that Pt electrodes are only sensitive to the conditions found in a few mm^3 connected to the Pt surface are valid, but from our perspective, only when the surrounding physical framework is kept in mind with the dynamic behaviour of ε_{CT_conn}.

4 | CONCLUSIONS

The soil redox status is relevant to obtain a mechanistic understanding of processes that take place under temporary water-saturated conditions, for example, greenhouse gas emission or mobilisation of distinct trace elements. Thus, the link to physical properties as the connective air-filled pore network is of great importance. We demonstrated that a small amount of ε_{CT_conn} of 0.02 $cm^3\ cm^{-3}$ is sufficient for our soil sample to determine the ecological relevant transition from reducing towards oxidising soil conditions as indicated by an increase in E_H. This threshold value is considerably lower than usual reports of ε close to 0.05 $cm^3\ cm^{-3}$ to represent sufficient aeration. Here, we showed the importance of pore functions (connectivity) rather than amount (porosity), especially in the near-saturated range. Non-invasive image analysis by µCT allowed us to link different pore networks to the redox status independently of the position of the electrode. Results presented here have to be taken carefully, as this is a pilot study with only one replication, thus it should be extended to a larger variety of substrates and soils, with larger sample sizes being mandatory to evaluate the likelihood of the soil being aerobic or anaerobic without the spatial restrictions associated to E_H measurements with Pt electrodes.

ACKNOWLEDGEMENTS

We greatly acknowledge the support of the mechanical workshop of the University Kassel to manufacture the plastic cylinder equipment. This research did not receive any specific grant from funding agencies in the public, commercial, or not-for-profit sectors.

Open access funding enabled and organized by Projekt DEAL.

AUTHOR CONTRIBUTIONS

Kristof Dorau: Conceptualisation (lead); writing – original draft (lead); writing – review and editing (lead). **Daniel Uteau:** Conceptualisation (lead); writing – original draft (lead); writing – review and editing (lead). **Maren Pia Hövels:** Formal analysis (lead); investigation (lead). **Stephan Peth:** Conceptualisation (lead); writing – review and editing (lead). **Tim Mansfeldt:** Conceptualisation (lead); writing – review and editing (lead).

DATA AVAILABILITY STATEMENT

The data that support the findings of this study are available from the corresponding author upon reasonable request.

ORCID

Kristof Dorau https://orcid.org/0000-0002-1815-1929
Daniel Uteau https://orcid.org/0000-0003-1499-4344
Maren Pia Hövels https://orcid.org/0000-0002-3116-9242
Stephan Peth https://orcid.org/0000-0001-9799-212X
Tim Mansfeldt https://orcid.org/0000-0002-7557-6827

REFERENCES

Bohn, H. L. (1971). Redox potentials. *Soil Science*, *112*, 39–45.

Carminati, A., Kaestner, A., Lehmann, P., & Flühler, H. (2008). Unsaturated water flow across soil aggregate contacts. *Advances in Water Resources*, *31*, 1221–1232.

Dorau, K., Luster, J., & Mansfeldt, T. (2018). Soil aeration: The relation between air-filled pore volume and redox potential. *European Journal of Soil Science*, *69*, 1035–1043.

Dorau, K., & Mansfeldt, T. (2016). Comparison of redox potential dynamics in a diked marsh soil: 1990 to 1993 versus 2011 to 2014. *Journal of Plant Nutrition and Soil Science*, *179*, 641–651.

Durner, W. (1994). Hydraulic conductivity estimation for soils with heterogeneous pore structure. *Water Resources Research*, *30*, 211–223.

Fiedler, S., Vepraskas, M. J., & Richardson, J. L. (2007). Soil redox potential: Importance, field measurements, and observations. In D. L. Sparks (Ed.), *Advances in agronomy* (pp. 1–54). Academic Press.

Fischer, D., Pagenkemper, S., Nellesen, J., Peth, S., Horn, R., & Schloter, M. (2013). Influence of non-invasive X-ray computed tomography (XRCT) on the microbial community structure and function in soil. *Journal of Microbiological Methods*, *93*, 121–123.

Flühler, H., Stolzy, L. H., & Ardakani, M. S. (1976). A statistical approach to define soil aeration in respect to denitrification. *Soil Science*, *122*, 115–123.

Gillespie, L. J. (1920). Reduction potentials of bacterial cultures and of water-logged soils. *Soil Science*, *9*, 199–216.

Glinski, J., & Stepniewski, W. (1985). *Soil aeration and its role for plants*. CRC Press.

IUSS Working Group WRB. (2015). *World reference base for soil resources 2014, update 2015*. FAO.

Keiluweit, M., Gee, K., Denney, A., & Fendorf, S. (2018). Anoxic microsites in upland soils dominantly controlled by clay content. *Soil Biology and Biochemistry*, *118*, 42–50.

Mansfeldt, T. (2003). In situ long-term redox potential measurements in a dyked marsh soil. *Journal of Plant Nutrition and Soil Science*, *166*, 210–219.

Mansfeldt, T. (2004). Redox potential of bulk soil and soil solution concentration of nitrate, manganese, iron, and sulfate in two gleysols. *Journal of Plant Nutrition and Soil Science*, *167*, 7–16.

Mehra, O. P., & Jackson, M. L. (1960). Iron oxide removal from soils and clays by a dithionite-citrate system buffered with sodium bicarbonate. *Clays and Clay Minerals*, *7*, 317–327.

Nakamura, K., Katou, H., Suzuki, K., & Honma, T. (2018). Air-filled porosity as a key to reducing dissolved arsenic and cadmium concentrations in paddy soils. *Journal of Environmental Quality*, *47*, 496–503.

Neal, A. L., Bacq-Labreuil, A., Zhang, X., Clark, I. M., Coleman, K., Mooney, S. J., Ritz, K., & Crawford, J. W. (2020). Soil as an extended composite phenotype of the microbial metagenome. *Scientific Reports*, *10*, 10649.

Otsu, N. (1979). A threshold selection method from gray-level histograms. *IEEE Transactions on Systems, Man, and Cybernetics*, *9*, 62–66.

Peth, S. (2014). Noninvasive quantification of 3D pore space structures in soils. In J. Gliński, J. Horabik, & J. Lipiec (Eds.), *Encyclopedia of agrophysics* (pp. 516–520). Springer.

Peth, S., Horn, R., Beckmann, F., Donath, T., Fischer, J., & Smucker, A. J. M. (2008). Three-dimensional quantification of intra-aggregate pore-space features using synchrotron-radiation-based microtomography. *Soil Science Society of America Journal*, *72*, 897–907.

Pot, V., Peth, S., Monga, O., Vogel, L. E., Genty, A., Garnier, P., Vieublé-Gonod, L., Ogurreck, M., Beckmann, F., & Baveye, P. C. (2015). Three-dimensional distribution of water and air in soil pores: Comparison of two-phase two-relaxation-times lattice-Boltzmann and morphological model outputs with synchrotron X-ray computed tomography data. *Advances in Water Resources*, *84*, 87–102.

Reddy, K. R., & DeLaune, R. D. (2008). *Biogeochemistry of wetlands - Science and applications*. CRC Press.

Rohe, L., Apelt, B., Vogel, H. J., Well, R., Wu, G. M., & Schlüter, S. (2021). Denitrification in soil as a function of oxygen availability at the microscale. *Biogeosciences*, *18*, 1185–1201.

Schwertmann, U. (1964). Differenzierung der Eisenoxide des Bodens durch Extraktion mit Ammoniumoxalat-Lösung. *Zeitschrift für Pflanzenernährung, Düngung, Bodenkunde*, *105*, 194–202 (in German).

Tippkötter, R., Eickhorst, T., Taubner, H., Gredner, B., & Rademaker, G. (2009). Detection of soil water in macropores of undisturbed soil using microfocus X-ray tube computerized tomography (μCT). *Soil and Tillage Research*, *105*, 12–20.

Uteau, D., Hafner, S., Pagenkemper, S. K., Peth, S., Wiesenberg, G. L. B., Kuzyakov, Y., & Horn, R. (2015). Oxygen and redox potential gradients in the rhizosphere of alfalfa grown on a loamy soil. *Journal of Plant Nutrition and Soil Science*, *178*(2), 278–287.

Wanzek, T., Keiluweit, M., Varga, T., Lindsley, A., Nico, P., Fendorf, S., & Kleber, M. (2018). The ability of soil pore network metrics to predict redox dynamics is scale dependent. *Soil Systems*, *2*, 1–25.

Whitfield, M. (1972). The electrochemical characteristics of natural redox cells. *Limnology and Oceanography*, *17*, 383–393.

Withers, P. J., Bouman, C., Carmignato, S., Cnudde, V., Grimaldi, D., Hagen, C. K., Maire, E., Manley, M., Du Plessis, A., & Stock, S. R. (2021). X-ray computed tomography. *Nature Reviews Methods Primers*, *1*, 1–18.

Yang, J., Hu, Y., & Bu, R. (2006). Microscale spatial variability of redox potential in surface soil. *Soil Science*, *171*, 747–753.

Zou, C., Penfold, C., Sands, R., Misra, R. K., & Hudson, I. (2001). Effects of soil air-filled porosity, soil matric potential and soil strength on primary root growth of radiata pine seedlings. *Plant and Soil*, *236*, 105–115.

SUPPORTING INFORMATION

Additional supporting information may be found in the online version of the article at the publisher's website.

How to cite this article: Dorau, K., Uteau, D., Hövels, M. P., Peth, S., & Mansfeldt, T. (2022). Soil aeration and redox potential as function of pore connectivity unravelled by X-ray microtomography imaging. *European Journal of Soil Science*, *73*(1), e13165. https://doi.org/10.1111/ejss.13165